Characterization of Optical Diffraction and Crystal Structure in Monodisperse Polystyrene Colloids

ROGER J. CARLSON* and SANFORD A. ASHER
Department of Chemistry, University of Pittsburgh, Pittsburgh, Pennsylvania 15260

Bragg diffraction of laser light from crystalline aqueous colloids of polystyrene spheres is examined to determine crystal structure, orientation, and elasticity. A new technique using Kossel rings is described which simultaneously measures structure, lattice spacings, and crystallite orientation. The monodisperse polystyrene sphere latex dispersions crystallize into large single crystals, which, depending on sphere concentration, are either face-centered or body-centered cubic. The interparticle spacings in the crystals are many times larger than the sphere diameter (0.109 μm). The use of tunable lasers to easily determine crystal structure is described, and the technique is further illustrated by the experimental determination of the bulk modulus. The bulk modulus is a macroscopic physical constant which can be used to monitor intersphere potentials and the screening of the particle charges by electrolytes in the solution. Data are presented which suggest that crystallite orientation occurs with the closest packed sphere layers parallel to the sample cell quartz walls.

Index Headings: Bragg Diffraction; Light scattering; Colloids; Polystyrene spheres; Latex.

INTRODUCTION

Significant interest exists in elucidating the structure and physical properties of colloids.[1,2] This interest stems from their industrial importance[3] as well as from the utility of some colloidal systems as models of liquid and solid structure,[4–9] and from their usefulness for studying phase transition phenomenology.[10–21] During the preceeding thirty years a number of groups have demonstrated that dispersions of charged macromolecules can adopt ordered crystalline structures.[22–33] Examples include proteins,[28] virus particles,[27] bacteria,[22] cell suspensions,[22] silver iodide particles and other sols,[22] and dispersions of polystyrene spheres.[4–21] The most studied colloid consists of a dispersion of monodisperse polystyrene latex spheres in various solvents such as water, methanol, benzene, etc. The polystyrene spheres are prepared by emulsion polymerization, and generally contain on the order of 2000 SO_4 functional groups per sphere.[34,35] The sphere diameters which have demonstrated crystalline ordering range from 200–10,000 Å. These spheres can be prepared as monodisperse samples with a sphere diameter relative standard deviation of less than 1%. The narrow size distribution has led to the use of these spheres as electron microscopy standards, and as substrates for clinical diagnostic tests.[3]

Due to the large number of negatively charged groups, the major intersphere interactions in these dispersions are screened coulombic repulsive interactions.[36–38] For low ionic strengths this repulsive interaction occurs over distances many times the sphere diameter.[36] Due to boundary conditions such as the solvent volume and gravitational settling forces[10,39] the spheres crystallize into an ordered array with intersphere spacings many times the sphere diameter. Lattice spacings can be comparable to the wavelength of visible light, and Bragg diffraction will occur, resulting in an iridescent sample which displays optical properties similar to those of high quality opals.[40]

The crystal structure of polystyrene sphere dispersions depends upon both the sphere concentration and the presence of electrolytes which screen the repulsive interactions.[29,41,42] Although previous studies of the polystyrene sphere crystals have led to an assignment of a face-centered cubic structure (FCC) for high sphere concentrations and a body-centered cubic structure (BCC) at low concentrations,[29] little consistent data have been presented to quantitatively demonstrate these assignments. Characterization of the crystal structure for various sample compositions and temperatures is required to determine the phase diagram of this system.[11,12,21,43] The importance of understanding the phase diagram has led to recent attempts to theoretically calculate the crystal ordering for spherical particles which interact with hard sphere repulsive interactions.[4,9,13,16–18,44] These calculations also attempt to demonstrate a theoretical understanding of the factors which determine crystal ordering in the nobel gas solids (which are important for matrix isolation techniques) and Wigner electron lattices.[9]

The polystyrene sphere colloids also undergo a phase transition between the solid-like crystalline lattice and an amorphous liquid-like structure lacking long-range order. This melting can be induced either by an increase in the electrolyte concentration[21,29] or by an increase in temperature.[11,12,43] A number of recent experimental and theoretical studies have begun to examine this transition. Significant interest exists in this portion of the

Received 12 June 1982.
* Present address: Department of Chemistry, University of Wisconsin–Madison, 1101 University Avenue, Madison, WI, 53706.

0003-7028/84/3803-0297$2.00/0

phase diagram because the polystyrene sphere colloids are useful for studying the solid-liquid phase transition phenomenon.

Any detailed understanding of the sphere interparticle interactions will require the determination of crystal physical parameters such as compressibility, elasticity, and the phonon mode frequencies.[45,46] These measurements of elasticity and compressibility require monitors of the crystal structure and lattice spacings. In this report we characterize the optical diffraction phenomena observed for polystyrene sphere crystals and illustrate the use of Kossel rings for deducing crystal structure. We also use this simple technique to reexamine the dependence of crystal structure and orientation on both sphere concentration and sample boundary conditions and illustrate utility of the Kossel ring technique by examining gravitational compression of the colloidal lattice in order to determine the crystal compressibility. Such measurements should provide useful empirical data for the theoretical evaluation of the interparticle potentials responsible for the ordering process.

After completion of this work we became aware of other observations of the Kossel ring phenomenon in the polystyrene sphere crystals,[31,45] and of a very recent extensive theoretical examination of the possible Kossel ring patterns in these crystals.[47] Our Kossel ring technique is experimentally easier than that of Pieranski *et al.*[47] and utilizes a minimum number Kossel ring technique which simplifies the analysis by utilizing a laser wavelength which diffracts the fewest Kossel rings required to uniquely define a crystal structure.

EXPERIMENTAL

Sample Preparation. Monodisperse polystyrene spheres were obtained from Dow Diagnostics (Lot number 1A90). The sphere diameter was indicated to be 0.109 μm with a standard deviation of 0.0027 μm. The latex dispersion was freed of electrolyte and surfactant impurities by dialysis against a bath of doubly distilled water containing mixed bed ion exchange resin. Dialysis occurred in a sealed glass flask over a three week period, with the dialysis bath exchanged daily. After the dialysis treatment the dispersion (approximately 10% by weight) was stored as a suspension over ion exchange resin. The exchange resin was supplied by Bio-Rad (Analytical Grade AG501-X8 mixed bed resin). Ion exchange resin has been reported to typically contain polyelectrolyte impurities. Thus, the resin was cleaned before use by using a procedure similar to that of Vanderhoff and Van Den Hul.[35] The resin was washed extensively using 85°C doubly distilled water, room temperature water, and reagent grade methanol. This procedure was repeated a total of three times.

The single crystal samples used for the studies reported here were prepared by diluting the polystyrene sphere suspensions with deionized, doubly distilled water in 1.5 mm i.d. quartz capillaries containing a small amount of ion exchange resin. Quartz was used to avoid the leaching of ions as is commonly found when using glass capillaries. After dilution the capillaries were sealed and placed in a room temperature water bath for several weeks during which time the samples crystallized, presumably, into their thermodynamically most stable crystal structure. This is further indicated by the reproducibility of the crystal structure observed between identically prepared samples.

Bragg Scattering Apparatus. Diffraction phenomena were measured using an apparatus similar to that of Williams and Crandall.[29] A cylindrical tank containing water (Fig. 1) was mounted on a rotating table and the sample capillary was suspended in the water bath on a rod coincident with the axis of the outer cylinder. The sample could be both translated along and rotated about the axis of the tank. The water tank was used to match the refractive index of the sample during measurements of the Bragg angles. This avoided correcting for refraction of the diffracted light. The diffraction spots and Kossel rings were recorded by tracing the observed patterns on tracing paper tightly wrapped around the exterior of the tank.

The sampling geometry used permitted an accurate positioning of the sample capillary at the center of the cylindrical tank. Diffraction of the laser light from the capillary was used to ensure that the capillary axis was parallel to that of the cylindrical tank. In view of these facts and because the entire Kossel ring pattern could be observed for laser powers greater than 50 mW, we estimate the relative errors in lattice spacings to be less than 2%. Diffraction phenomena were excited by using a Spectraphysics model 164 Ar^+ laser, or by using a Spectraphysics Model 375 tunable jet stream dye laser. For samples with large lattice spacings, longer wavelength light from the dye laser was used to identify the crystal structure; the Kossel ring pattern was simplied by limiting the Bragg scattering to only the largest lattice spacings.

RESULTS AND DISCUSSION

Irradiation of the ordered polystyrene latex dispersions with light of shorter wavelength than twice the crystalline lattice spacing leads to Bragg diffraction. In the case of a sample within a capillary in the apparatus shown in Fig. 1, Bragg spots appear at angles 2θ to the laser beam propagation direction when a lattice plane is at an angle $\theta = \sin^{-1} n\lambda/2d$. In the case of one large crystallite it is possible to determine the crystal structure by carefully rotating the sample within the beam and collecting data on lattice spacings and relative lattice plane orientations. Since the crystallite orientation is not known initially this procedure can be quite tedious.

However, a much easier technique is available which utilizes the Kossel rings which result from the inability of light in the sample to propagate along directions which fulfill the Bragg condition.[48] A series of such rings accompany the Bragg diffraction spots and are displayed on the target screen as shown in Fig. 1. The Kossel rings are the loci of dark lines resulting from the intersection of surfaces of cones with the cylindrical screen around the sample chamber. The apex of each cone originates within the samples. For laser powers greater than 50 mW the Kossel rings dominate the scattering pattern. The rings simultaneously specify both the lattice plane spacings and their orientation. Kossel rings have been recognized for the past 50 years and have been used for

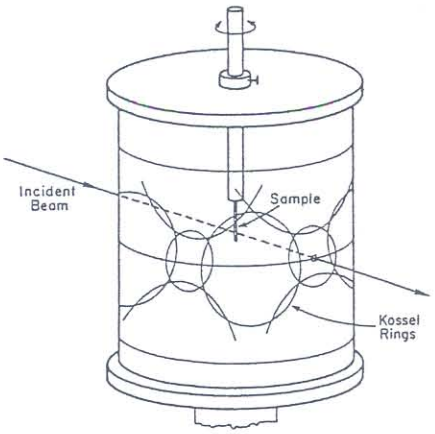

Fig. 1. Experimental apparatus showing Kossel ring patterns.

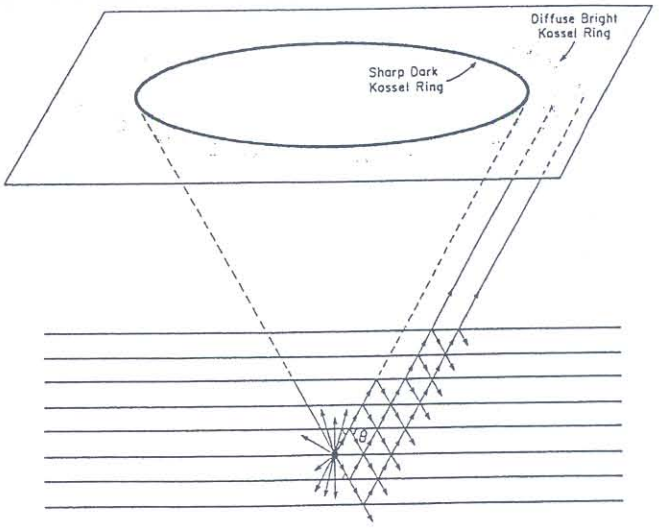

Fig. 2. Formation of bright and dark Kossel rings. Isotropic scattering of the laser light results in a divergent light source within the sample. The light at the Bragg angle θ is diffracted and cannot propagate through the lattice. Thus, dark Kossel rings are projected onto a target screen. The bright Kossel rings are considerably broadened by multiple Bragg diffraction.

high resolution x-ray studies of crystalline materials, especially for metals.[48] Figure 2 demonstrates the origin of these rings.

In order to observe these rings a divergent source of radiation is used. For x-ray diffraction the sample itself can be used as the electron impact target for producing the x-rays. In our case a divergent source derives from isotropic scattering of the laser light by the polystyrene spheres. Thus, a source of radiation is generated at the sample surface and within the sample interior. In the absence of crystalline lattice planes this radiation would be essentially isotropic, leading to a relatively uniform illumination of a target screen situated around the sample. However, each set of lattice planes will diffract radiation which attempts to propagate at the Bragg angle. This radiation is diffracted away and the loci of these directions are surfaces of cones whose axes are normal to the diffracting planes. When these cones are projected onto a target spherically symmetric around the sample, dark circles (deficiency lines) are observed.[47,48] In contrast, ovals are generated for the cylindrical target used in our study.

The lattice spacing of the set of planes producing the Kossel ring can be calculated from the angular width of the Kossel ring, δ, by the modified Bragg equation $n\lambda = 2d \cos \delta/2$, where λ is the wavelength of light within the sample compensated for the sample refractive index, μ ($\lambda = \lambda_o/\mu$). d is the lattice spacing and n is an integer. Analysis of sizes of the rings, their number, and their pattern determines the crystal structure, lattice spacings and orientation.

Bragg diffraction of the divergent light can also result in bright Kossel rings concentric with the dark rings (Fig. 2). This effect is often observed in divergent beam x-ray studies of common materials. However, in our samples bright rings are seldom observed due to the intense scattering power of the spheres which multiply diffract away the light responsible for the bright rings. However, we typically observed bright rings in thin polystyrene sphere samples (25 μm), or, if the capillary samples are illuminated, at the capillary edge. This occurs because fewer layers are traversed as the light leaves the sample. The intense scattering power of the spheres derives from the dielectric constant difference between the spheres and the adjacent water layers. This difference is much greater than the dielectric constant variation normally encountered for x-rays in a material. Indeed the difference in scattering power results in the inability of the usual "kinematic" x-ray diffraction theory to account for the intensities, widths, and exact angles for the Bragg diffraction phenomena. In the case of polystyrene sphere crystals, the diffraction phenomena are best described by "dynamical" x-ray theory.[49,50] As earlier recognized by Hiltner and Krieger,[15] the intense scattering by the layers of spheres close to the source depletes the beam traveling through the sample. In the x-ray literature this is known as "primary extinction." It should be noted that this phenomenon derives from diffraction and is distinctly different from absorption which is specified by the x-ray mass absorption coefficient. Indeed the magnitude of primary extinction can be significantly greater than normal x-ray absorption. The fact that attenuation of the beam passing through the sample has to be included in calculating the Bragg angles, widths, and intensities is the basis of the difference between kinematic and dynamical x-ray theory. In general the Bragg angles will be close to that specified by kinematic theory. However, the intensities and widths may be dramatically different, and new phenomena, such as anomalous transmission (Borrmann effect), may occur.[40]

The observed Kossel ring patterns can be matched with those predicted by theory in order to unambiguously determine structure and orientation. The angles, ϕ, between the axes of the cones corresponding to the crystal planes with Miller indices $(h_1k_1l_1)$ and $(h_2\ k_2\ l_2)$ for face-centered cubic (FCC), body-centered cubic (BCC), and hexagonal close-packed (HCP) structures can be calculated as follows,

FCC and BCC:

$$\cos \phi = \frac{h_1h_2 + k_1k_2 + l_1l_2}{\sqrt{h_1^2 + k_1^2 + l_1^2}\sqrt{h_2^2 + k_2^2 + l_2^2}}$$

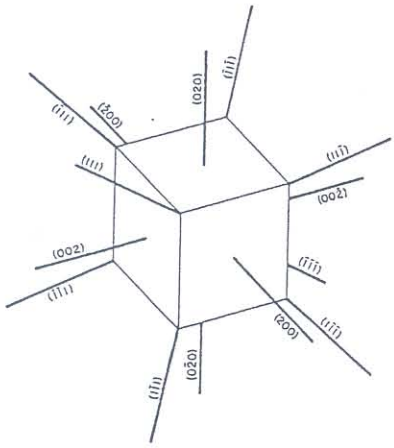

(a)

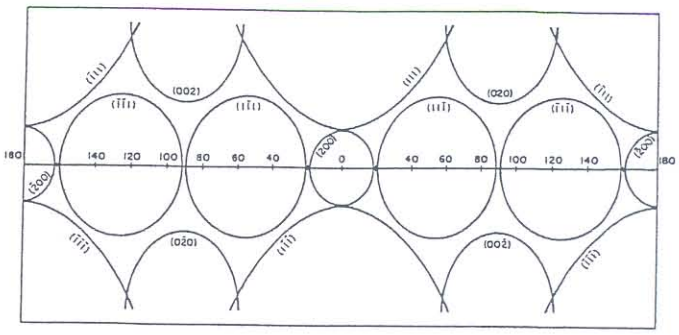

(b)

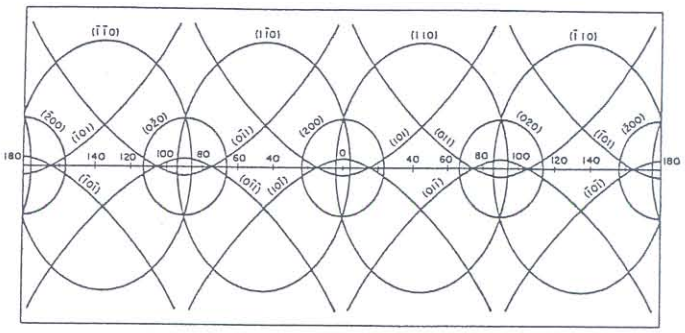

(c)

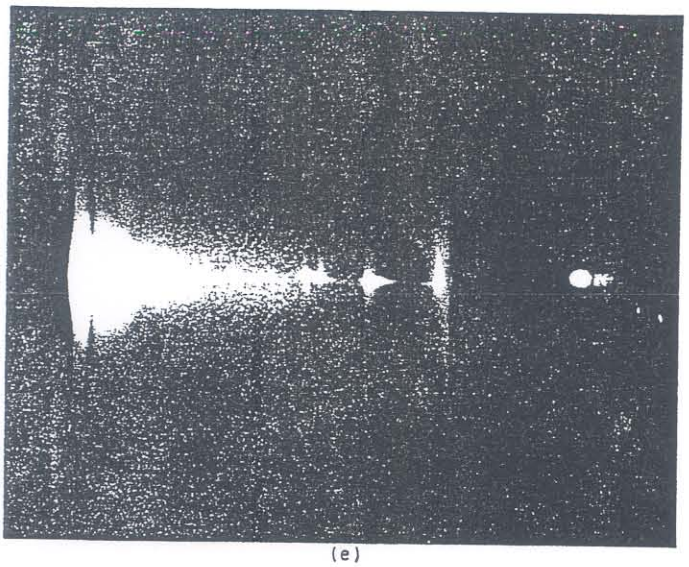

(e)

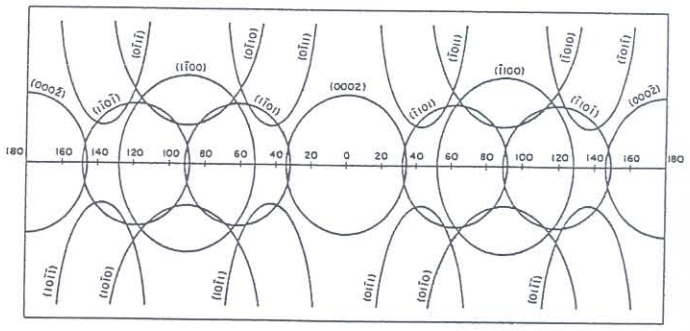

(d)

Fig. 3. Kossel ring patterns on cylindrical screen of radius 9.05 cm for $\lambda = 5000$ Å. a) Geometry of Kossel ring formation from a FCC lattice. Each set of lattice planes results in a Kossel ring whose axis is perpendicular to the lattice planes. These axes are shown by the normals to the planes which are labeled by their Miller indices. Calculated Kossel rings from: b) face-centered cubic lattice, $N = 6.37 \times 10^{13}$ spheres/cc; c) body-centered cubic lattice, $N = 2.83 \times 10^{13}$ spheres/cc; d) hexagonally close-packed lattice, $N = 6.22 \times 10^{13}$ spheres/cc. The angles along the meridian are listed along the center line of each figure. e) Photograph of Kossel ring pattern from FCC structure using apparatus shown in Fig. 1.

HCP:

$$\cos\phi = \frac{\frac{2}{3}(2h_1 + k_1)(2h_2 + k_2) + 2k_1k_2 + \frac{3}{4}l_1l_2}{\sqrt{\frac{2}{3}(2h_1 + k_1)^2 + 2k_1^2 + \frac{3}{4}l_1^2} \cdot \sqrt{\frac{2}{3}(2h_2 + k_2)^2 + 2k_2^2 + \frac{3}{4}l_2^2}}$$

Also, lattice spacings d_{hkl} and structure factors (S) are given by,

FCC:

$$|S|^2 = f^2\{[1 + \cos\pi(h + k) + \cos\pi(h + l) + \cos\pi(k + l)]^2 + [\sin\pi(h + k) + \sin\pi(h + l) + \sin\pi(k + l)]^2\}$$

$$d_{hkl} = \frac{\sqrt{2}d}{\sqrt{h^2 + k^2 + l^2}}$$

BCC:

$$|S|^2 = f^2[2 + 2\cos\pi(h + k + l)]$$

$$d_{hkl} = \frac{2d}{\sqrt{3(h^2 + k^2 + l^2)}}$$

HCP:

$$|S|^2 = f^2[2 + 2\cos 2\pi(\tfrac{2}{3}h + \tfrac{1}{3}k + \tfrac{1}{2}l)]$$

$$d_{hkl} = \frac{d}{\sqrt{\frac{1}{3}(2h + k)^2 + k^2 + \frac{3}{8}l^2}}$$

where f is the scattering factor of each sphere and d is the interparticle spacing. Table I shows some calculated values. The magnitude of the structure factor qualitatively specifies the intensity of the Bragg diffraction spots and the darkness of the Kossel rings. For dynamical dif-

TABLE I. Calculated values of the structure factor, S, for the 10 largest interplane spacings of the face-centered cubic (FCC), body-centered cubic (BCC), and hexagonal close-packed (HCP) lattices. The structure factors are expressed as $|S|^2/f^2$, where f is the scattering factor. d_{hkl}/d is the ratio of the interplane spacing to the nearest neighbor interparticle spacing, d.

FCC			BCC		
hkl	$\frac{\lvert S\rvert^2}{f^2}$	$\frac{d_{hkl}}{d}$	hkl	$\frac{\lvert S\rvert^2}{f^2}$	$\frac{d_{hkl}}{d}$
100	0	1.4142	100	0	1.1547
110	0	1.0000	110	4	0.8165
111	16	0.8165	111	0	0.6667
200	16	0.7071	200	4	0.5774
210	0	0.6325	210	0	0.5164
211	0	0.5774	211	4	0.4714
220	16	0.5000	220	4	0.4082
300, 211	0	0.4714	300, 211	0	0.3849
310	0	0.4472	310	4	0.3651
311	16	0.4264	311	0	0.3482

HCP		
hkl	$\frac{\lvert S\rvert^2}{f^2}$	$\frac{d_{hkl}}{d}$
001	0	1.6330
010, 100	1	0.8660
002	4	0.8165
011, 101	3	0.7651
102, 012	1	0.5941
003	0	0.5443
110	4	0.5000
111	0	0.4781
013, 103	3	0.4609
200, 020	1	0.4330

fraction phenomenon, however, careful account also has to be taken of beam attenuation, which is intimately related to the sphere scattering power, and to the relative crystal perfection. For planes with a structure factor of zero Bragg diffraction is not allowed nor observed.

By calculations such as those described above it is easy to determine the pattern of Kossel rings which could be observed. Figure 1 shows the formation of a ring pattern in our apparatus and Fig. 3 shows patterns calculated for FCC, BCC, and HCP structures. For the ring patterns in Fig. 3 the (011) FCC, (001) BCC and (110) HCP planes were chosen to be perpendicular to the cylindrical axis of the scattering chamber. This orientation was chosen mainly because it is consistent with the experimental observations (Fig. 3e) to be discussed below. Note also that four Miller indices ($hkil$) are used for the HCP structure, where i is defined as $-(h + k)$. This convention derives from the fact that one can choose two equivalent but distinct hexagonal unit cells for this structure.[51] Table I lists the 10 largest lattice spacings of the three crystal structures. If the laser wavelength is shorter than twice the distance between a set of high Miller index planes, these planes as well as all sets of planes with lower Miller indices will contribute Kossel rings. This will clearly result in a complex, difficult-to-interpret pattern. We utilize a dye laser to select a wavelength which will result in the minimum number of Kossel rings required to uniquely define a crystal structure. This significantly aids the assignment of the crystal structure and is essential where crystal twinning or microcrystals exist, in which case it is necessary to separate

TABLE II. Concentration dependence of crystal structure for polystrene sphere samples.

Sample	N (cm^{-3})	w	d(Å)	Structure
A	$(7.08 \pm 0.18) \times 10^{13}$	0.050 ± 0.007	2713 ± 23	FCC
B	$(5.43 \pm 0.08) \times 10^{13}$	0.038 ± 0.006	2964 ± 14	FCC
C	$(3.40 \pm 0.15) \times 10^{13}$	0.024 ± 0.004	3370 ± 50	BCC
D	$(1.26 \pm 0.05) \times 10^{13}$	0.0090 ± 0.0014	4680 ± 70	BCC

Where: $d_0 = 1090 \pm 40$ Å; $\rho = 1.045$; $\mu = 1.33$.

the Kossel patterns from each crystal. Once a crystal structure is postulated from a series of one or two Kossel rings the laser wavelength can be decreased to bring in more Kossel rings to confirm the structure. Wavelength tunability is also essential if one wishes to examine a large range of polystyrene latex concentrations.

Table II lists the samples used for the crystal structure and orientation measurements. The table indicates the sphere concentration of each sample within the irradiated volume, the nearest neighbor spacing, and the crystal structure. The sphere concentrations listed represent the calculated concentration within the capillary tube at the point where diffraction is measured (*vide infra*); gravitational forces cause a distribution of sphere concentration along the tube axis with a small relative compression occurring towards the bottom of the capillary. Sphere concentrations were determined at the observation point within the sample using the expressions HCP and FCC:

$$N = \frac{\sqrt{2}}{d^3}, \qquad w = \frac{\rho}{\frac{3\sqrt{2}}{\pi}\left(\frac{d}{d_0}\right)^3 + \rho - 1}$$

BCC:

$$N = \frac{3\sqrt{3}}{4d^3}, \qquad w = \frac{\rho}{\frac{8}{\pi\sqrt{3}}\left(\frac{d}{d_0}\right)^3 + \rho - 1}$$

where N is the number of spheres per cm^3, w is the weight fraction, d is the measured interparticle spacing, ρ is the ratio of the density of polystyrene to that of water (taken as 1.045), and d_0 is the diameter of the spheres (0.109 μm). This is a more accurate representation of sphere concentration than that calculated from the dilution factor, both because of gravitational compression and because the ion exchange resin typically swells and absorbs water, concentrating the sphere suspension in the capillaries.

We observe both FCC and BCC crystal structures in the capillary cells. As previously reported,[29] the FCC structure is observed at high sphere concentrations and a BCC structure is observed at low concentrations. However, we observe a BCC structure at significantly higher concentrations than previously reported.[14,25,47] As Table II shows, the BCC structure is observed at concentrations as high as 3.4×10^{13} spheres/cc or 2.4 weight percent polystyrene. The origin of this discrepancy is not clear. However, it could result from electrolyte or other sample inhomogeneities. This possibility is supported by Pieranski *et al.*[47] who, while never observing the pres-

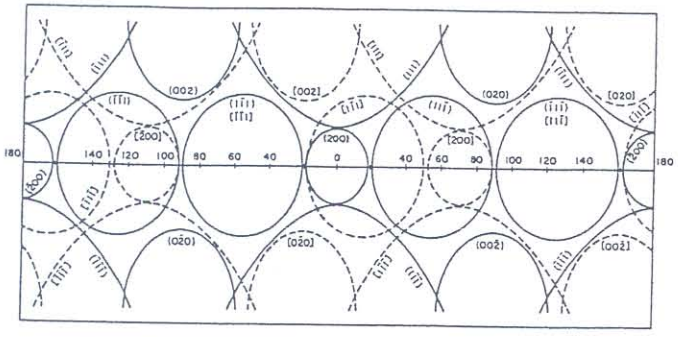

Fig. 4. Two dimensional sketch of Kossel ring pattern from twinned face-centered cubic crystal.

ence of a FCC lattice alone, occasionally observed coexistence of the FCC and BCC lattices.

In order to put these observations into the context of a phase diagram it is necessary to specify electrolyte concentration. We have extensively dialyzed the spheres and measured them in the presence of ion exchange resin. Thus, we assume that the normal exogenous electrolyte concentration is zero.

We have never observed the HCP structure in the capillary cells. However, in studies of thin samples (25 μm) between flat quartz plates we have seen evidence of hexagonal structure. The evidence derives from the hexagonal symmetry of the Kossel rings. These cells also have shown crystal structures which were clearly not HCP but may have been FCC or BCC. We are continuing our investigation into these thin samples in order to determine the effect of sample boundary on crystal structure and orientation (however, *vide infra*).

As indicated earlier the (011) FCC and (001) BCC layers were generally perpendicular to the capillary axis. Thus, there appears to be crystal orientation induced by the sample container, as noted previously by Luck *et al.*[22] and subsequently confirmed by Clark *et al.*[31] From experiments using a hemispherical cell illuminated through the flat surface Luck *et al.* suggested that the Bragg diffraction data indicated that the FCC (111) planes immediately adjacent to the glass plates were oriented parallel to the glass surface. Our data using Kossel rings monitor orientation in the bulk rather than primarily at the sample surface, and is consistent with the previous assignment of FCC crystallite orientation. However the Kossel ring data in the cylindrical cells cannot distinguish conclusively whether the (111) or (100) planes of the FCC lattice are parallel to the surface. We also find that either the (110) or (100) BCC planes lie parallel to the glass surface. We are presently examining this orientation in thin samples contained between two parallel quartz plates to discriminate between the two possibilities. It is interesting that the HCP structure tentatively observed in the thin cells had their (001) planes parallel to the glass surfaces. The FCC (111), the BCC (110), and the HCP (001) planes each derive from those planes containing the highest density of spheres. This may suggest that the sample orientation is due to strong attractive interactions between the quartz substrate and the spheres.

Although the samples we prepare generally consist of large single crystals which fill the cross-sectional area of the capillary and extend for distances of 1 cm to 10 cm, we often observe crystal twinning in the FCC structure. Crystal twinning was previously reported for the BCC structure in these systems.[47] Figure 3e shows a photograph and Fig. 4 an accurate sketch of the Kossel ring pattern for a sample in which two FCC crystallites are twinned. From the Kossel ring pattern it is obvious that the two crystal orientations differ by only a rotation of one crystal by approximately 70° along the (011) axis (i.e., along the axis of the sample capillary).

TABLE III. Experimentally determined isothermal compressibility (β) and bulk modulus (B) for samples from Table II.

Sample	B(dyne/cm^2)	β(cm^2/dyne)
A	36 ± 6	0.028 ± 0.004
B	29 ± 5	0.035 ± 0.006

We have also utilized the Kossel ring technique to determine elastic constants for our single crystal samples as a function of sphere concentration and crystal structure. These results will be described in detail in a separate publication. However, we include some of these results here to demonstrate the utility of the Kossel technique.

Crandell and Williams[39] measured the Youngs elastic modulus for a BCC structure by monitoring the gravitational compression of polystyrene sphere samples. We have utilized the Kossel ring techniques to measure an analogous elastic constant, the bulk modulus B for *single crystal samples* in the face-centered cubic structure. The bulk elastic modulus was determined by measuring the lattice spacings as a function of position along the capillary axis. This measurement was accomplished by measuring the Kossel ring diameter as the sample capillary was accurately translated along its axis through the laser beam. The crystal structure and orientation were simultaneously monitored, and no change was observed. We assume an isotropic compression of the lattice. Thus, the bulk modulus is defined as

$$B = -V\left(\frac{\partial P}{\partial V}\right)_T$$

where B is the reciprocal of the isothermal compressibility β. V is the volume of the unit cell as monitored from the Kossel ring pattern and P is the effective gravitational pressure,

$$P = \int \frac{4mg}{V}\, dz$$

or

$$\left(\frac{\partial P}{\partial z}\right)_T = \frac{4mg}{V}$$

where m is the effective mass of a polystyrene sphere in water calculated from the volume and the density difference between polystyrene and water (i.e., 1.045 gm/cc and 1.000 gm/cc, respectively). $m = (3.1 \pm 0.5) \times 10^{-17}$ gm. g is the gravitational acceleration and z is the vertical position in the capillary.

Since

$$\frac{-dP}{dz} = \frac{B}{V}\frac{dV}{dz}$$

integrating with respect to z yields (assuming B as constant)

$$V = \frac{-4mg}{B}(z - z_0) + V_0.$$

Where V_0 is the unit cell volume at $z = z_0$ (any arbitrary reference point in the sample). Figure 5 shows a plot of V vs. $(z - z_0)$ whose slope gives B. Table III lists the values of B and β measured for samples A and B from Table II.

As Williams and Crandall[39] pointed out, the compressibility values are extraordinarily low for these systems when one considers that an ideal gas of the same particle concentration would have a B of ~3 dyne/cm². The larger B for the polystyrene spheres results from the coulombic repulsive interactions. Measurements of B as a function of interparticle spacing and electrolyte concentration will result in new data on the electrical double layer and ionic screening in solutions.

The Kossel ring technique is ideal for these types of studies because in addition to accurately monitoring lattice spacings, the Kossel ring pattern determines crystal structure and orientation. In addition, careful measurements of the angles between Kossel rings easily determine anistropic compression within these samples. A more extensive report on the elastic measurements is in preparation.

CONCLUSIONS

The polystyrene sphere colloids are ideal systems for studying interactions between ionic species in solution. The strong Bragg diffraction of visible light from these macroscopically ordered systems illustrate all of the Bragg diffraction phenomenon normally encountered in x-ray diffraction studies. However, the strong scattering of the polystyrene spheres requires dynamical diffraction theory to account for the diffraction intensities and widths.

The Kossel ring technique permits simple measurements of interparticle spacing. Measurements of the compressibility indicate, as expected, that it increases with interparticle spacing. Since the compressibilities of these systems are controlled by the screened coulombic repulsive interaction between spheres, measurements of the compressibility as a function of sphere concentration and ionic strength will result in new information on ionic interactions, the electrical double layer, and the Debye screening length for ions in solution.

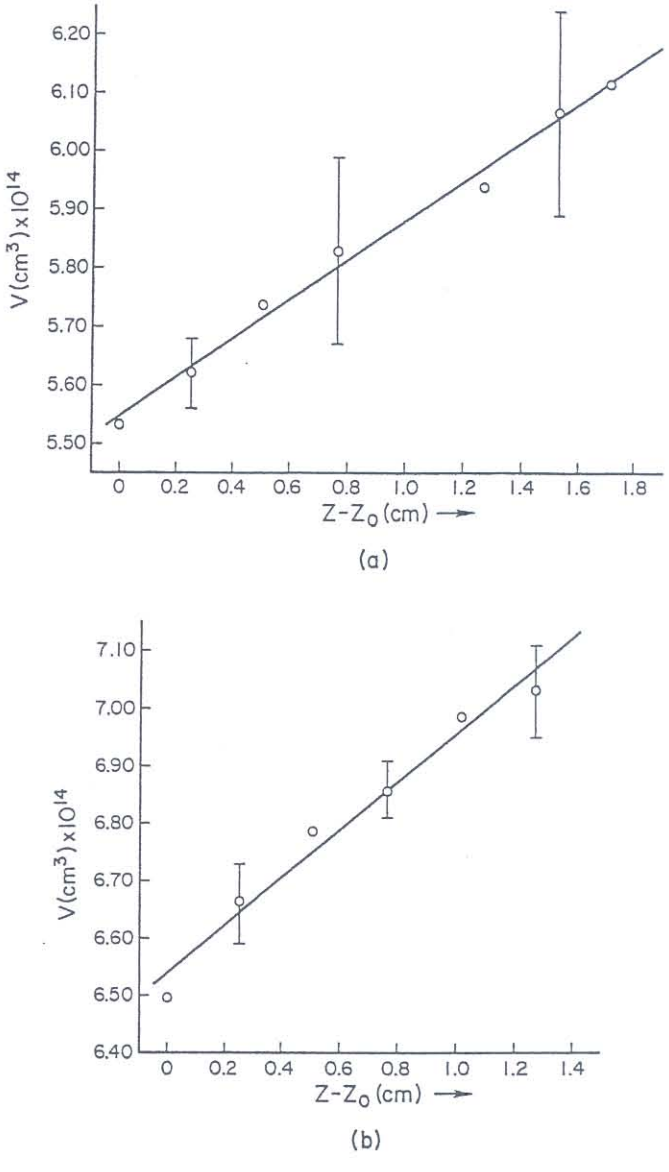

Fig. 5. Plot of unit cell volume vs. position in capillary for determination of compressibility for samples from Table II. a) Sample A. b) Sample B.

ACKNOWLEDGMENTS

We would like to gratefully acknowledge helpful discussions with Robert Meyer from the physics department of Brandeis University and technical assistance from James Patterson. We also thank Hana Novak, for her graphical skills and help.

The instrumentation used for this work was obtained from starter grant support from the Health Research and Services Foundation, Pittsburgh, Pennsylvania; BRSG Grant 2S07 RR07084-16 awarded by the Biomedical Research Support Grant Program, Division of Research Resources, National Insitutes of Health; a grant from the Petroleum Research Fund; and a Cottrell Research Grant from Research Corporation. Partial support for this work derived from NIH grant 1 R01 GM 30741-01.

1. N. Ise and T. Okubo, Acc. Chem. Res. **13**, 303 (1980).
2. M. Ed Kerker, *Colloid and Interface Science* (Acad. Press, New York, 1976) Vol. IV.
3. B. R. Bhattacharyya and B. D. Halpern, Polymer News **4**, 107 (1977).
4. D. W. Shaefer, J. Chem. Phys. **66**, 3980 (1977).
5. K. Takano and S. Hachisu, J. Phys. Soc. Jap. **42**, 1775 (1977).
6. A. Vrij, E. A. Nieuwenhuis, H. M. Fijnaut, and W. G. M. Agterol, Faraday Disc. **65**, 101 (1978).
7. J. C. Brown, P. N. Pusey, J. W. Goodwin, and R. H. Ottewill, J. Phys. (A.) **8**, 664 (1975).
8. W. Van Megen and I. Snook, J. Chem. Phys. **66**, 813 (1977).
9. J. M. Silva and B. J. Mokross, Solid State Comm. **33**, 493 (1980).
10. M. Wadati and M. Toda, J. Phys. Soc. Jap. **32**, 1147 (1972).
11. R. Williams, R. S. Crandall, and P. J. Wojtowicz, Phys. Rev. Lett. **37**, 348 (1976).
12. D. W. Shaefer and B. J. Ackersen, Phys. Rev. Lett. **35**, 1448 (1975).

13. I. Snook and W. van Megen, J. Chem. Soc., Faraday Trans. II, **72**, 216 (1976).
14. K. Takano and S. Hachisu, J. Chem. Phys. **67**, 2604 (1977).
15. S. Hachisu and Y. Kobayashi, J. Colloid Int. Sci. **46**, 470 (1974).
16. R. Hastings, J. Chem. Phys. **68**, 675 (1978).
17. S. L. Brenner, J. Phys. Chem. **80**, 1473 (1976).
18. S. Marcelja, D. J. Mitchell, and B. W. Ninham, Chem. Phys. Lett. **43**, 353 (1976).
19. A. Kose and S. Hachisu, J. Colloid Int. Sci. **46**, 460 (1974).
20. C. J. Barnes, D. Y. C. Chan, D. H. Everett, and D. E. Yates, Chem. Soc. Faraday Trans. II, **74**, 136 (1978).
21. S. Hachisu, Y. Kobayashi, and A. Kose, J. Colloid Int. Sci. **42**, 342 (1973).
22. V. W. Luck, M. Klier, and H. Wesslau, Naturwissenshaften **50**, 485 (1963).
23. T. Alfrey, E. B. Bradford, J. W. Vanderhoff, and G. Oster, J. Opt. Soc. Am. **44**, 603 (1954).
24. I. M. Krieger and F. M. O'Neill, J. Am. Chem. Soc. **90**, 3114 (1968).
25. P. A. Hiltner and I. M. Krieger, J. Phys. Chem. **73**, 2386 (1969).
26. P. A. Hiltner, Y. S. Papir, and I. M. Krieger, J. Phys. Chem. **75**, 1881 (1971).
27. K. M. Smith and R. Williams, Endeavor **17**, 12 (1958).
28. D. P. Riley and G. Oster, Discuss, Faraday Soc. **11**, 107 (1951).
29. R. Williams and R. S. Crandall, Phys. Lett. **48A**, 225 (1974).
30. J. W. Goodwin, R. H. Ottewill, and A. Parentich, J. Phys. Chem. **84**, 1580 (1980).
31. N. A. Clark, A. J. Hurd, and B. J. Ackerson, Nature **281**, 57 (1979).
32. H. Fujita, K. Ametini, and M. Inoue, RCA Reviews **36**, 108 (1975).
33. I. M. Krieger and P. A. Hiltner, *Polymer Colloids*, R. M. Fitch Ed., Plenum, New York (1975).
34. J. W. Vanderhoff, Pure Appl. Chem. **52**, 1263 (1980).
35. J. W. Vanderhoff and H. J. Van Den Hul, J. Macromol. Sci-Chem. **A7**, 677 (1973); J. Colloid Int. Sci. **28**, 336 (1968).
36. L. Barclay, A. Harrington, and R. H. Ottewill, Kooloid-Z,z. Polymere **250**, 655 (1972).
37. R. H. Ottewill, Prog. Colloid and Polymer. Sci. **67**, 71 (1980).
38. A. Watillon and A.-M. Joseph-Petit, Disc. Faraday Soc. **42**, 143 (1966).
39. R. S. Crandall and R. Williams, Science **198**, 293 (1977).
40. J. V. Sanders, Nature **204**, 1151 (1964).
41. K. Takano and S. Hachisu, J. Colloid Int. Sci. **66**, 124 (1978).
42. M. K. Udo and M. F. deSouza, Solid State Comm. **35**, 907 (1980).
43. C. Cowell and B. Vincent, J. Colloid Int. Sci. **87**, 518 (1982).
44. R. P. Keavey and P. Richmond, J. Chem. Soc. Faraday Trans, II, **72**, 773 (1976).
45. E. Dubois-Violette, P. Pieranski, F. Rothen, and L. Strzelecki, J. de Physique **41**, 369 (1980).
46. S. Mitaku, T. Ohtsuku, K. Enari, A. Kishimoto, and K. Okano, Jap. J. Appl. Phys. **17**, 305 (1978).
47. P. Pieranski, E. Dubois-Violetti, F. Rothen, and L. Strzelecki, J. de Physique **42**, 53 (1981).
48. K. Lonsdale, Phil. Trans. Royal Soc. (London) A, **240**, 219 (1947).
49. S. W. Wilkins, Phil. Trans. Royal Soc. (London) A, **299**, 275 (1981).
50. B. W. Balterman and H. Cole, Rev. Mod. Phys. **36**, 681 (1964).
51. A. Taylor, *X-ray Metallography* (John Wiley & Sons, Inc., New York 1961).